ISSN 1225-1089

Volume 50 Number 1, February 2013

KFS

he Korean Fiber Society

Textile Science and Engineering

한국섬유공학회지

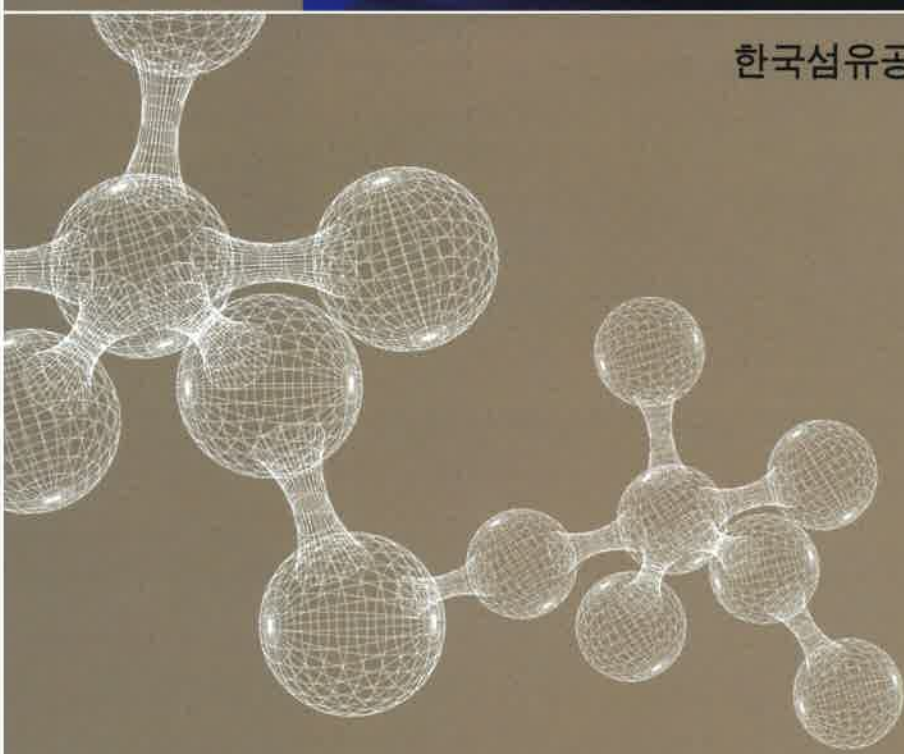

한국섬유공학회지 발간 50주년 기념 특집호

Formerly Journal of The Korean Fiber Society

한국섬유공학회지, 제50권 제1호 2013년 http://dx.doi.org/10.12772/TSE.2013.50.016

<연구논문>

태양전지 적용을 위한 poly(oligothiophene-*alt*-benzothiadiazole)s의 합성과 특성 분석

이윤규 · 정재웅 · 조원호†
서울대학교 재료공학부
(2012. 12. 25. 접수/2013. 1. 31. 채택)

Synthesis and Characterization of Low-bandgap Poly(oligothiophene-*alt*-benzothiadiazole)s for Photovoltaic Application

Yoonkyoo Lee, Jae Woong Jung, and Won Ho Jo†
Department of Materials Science and Engineering, Seoul National University, Seoul 151-742, Korea
(Received December 25, 2012/Accepted January 31, 2013)

Abstract: Two kinds of low-bandgap alternating copolymers composed of thiophene and benzothiadiazole were synthesized via the Stille coupling reaction. The effect of number of alkyl groups attached to oligothiophenes in the repeating unit of the copolymers on their optical, electrochemical, and photovoltaic properties was systematically investigated. One of the new polymers, poly(3,3"-dihexyl-2,2':5',2"-terthiophene-*alt*-2,1,3-benzothiadiazole) (**P1**), has better intermolecular packing than the other poly(3,3',3"-trihexyl-2,2':5',2"-terthiophene-*alt*-2,1,3-benzothiadiazole) (**P2**), and thus **P1** is more beneficial for achieving high charge carrier mobility. **P1**-based device shows the power conversion efficiency as high as 2.19% when blended with [6,6]-phenyl-C_{71}-butyric acid methyl ester after thermal treatment at 170 °C for 30 min.

Keywords: *polymer solar cell, low band-gap polymer, intermolecular packing*

1. Introduction

Bulk heterojunction (BHJ) polymer solar cells, fabricated by simple blending of an electron-donating conjugated polymer and an electron-accepting fullerene derivatives, have been reported to increase their performance continuously over the last decade [1-4]. Regioregular poly(3-hexylthiophene) (P3HT) blended with [6,6]-phenyl-C_{61}-butyric acid methyl ester ($PC_{61}BM$) was the first compound to reach the power conversion efficiency (PCE) as high as 5% [5,6]. Although possessing several advantageous properties, P3HT has a relatively wide bandgap of 1.9 eV and thus harvests photons only up to 22% of available solar photons. To absorb photons at longer wavelengths, where more photon flux is found from the emission of the sun, development of low-bandgap polymers is strongly required.

In recent years, low-bandgap polymers based on internal electron donor-acceptor (D-A) interaction have attracted great interest because their electronic properties can easily be tuned and their absorption ranges can be extended to longer wavelengths [7-10]. Following this approach, the D-A type copolymers based on electron-deficient benzothiadiazole and electron-rich aromatic compounds such as thiophene, carbazole, and benzodithiophene have been synthesized by several groups [11-13]. Very recently, a promising result has been reported by Heeger and co-workers using carbazole and benzothiadiazole moieties as building blocks of copolymers, demonstrating the PCE exceeding 6% [14].

Along with the light-harvesting ability, high charge mobility of conjugated polymers is also important for improving the performance of polymer solar cells. In order to exhibit good charge transport property, the polymer chains are required to pack closely each other facilitating charge transport through intermolecular hopping. Although most of solution-processable conjugated polymers have flexible side groups for solubility in organic solvents, the side groups very often prevent the polymer backbone from close packing. Hence, the enhancement of charge carrier mobility owing to close chain packing may have a trade-off with the solubility. To achieve both good solubility and high charge carrier mobility of conjugated polymers, much effort has been devoted to molecular design and synthesis of new polymers. However, there have been only a few reports on solution-processable low-bandgap polymers with high mobility [15,16], and the structure-property relation of the conjugated polymers is not fully explored [17-19].

Herein we report the synthesis of low-bandgap copolymers composed of thiophene and benzothiadiazole with fine-tuning of the number of solubilizing side groups, and their optical, structural, and photovoltaic properties. This paper also demonstrates that low-bandgap polymer with high

† Correspondence to Won Ho Jo (whjpoly@snu.ac.kr)
 1225-1089/2013-1/016-09

degree of interchain packing can be obtained by rational design of the number of substituent on the polymers.

2. Experimental

2.1. Materials

All reagents were obtained from Aldrich unless otherwise specified and used as received. Tetrahydrofuran (THF) was dried over sodium/benzophenone under nitrogen and freshly distilled before use. Toluene was dried over calcium hydride under nitrogen and freshly distilled prior to use. 4,7-Dibromo-2,1,3-benzothiadiazole (**1**) [20], 2-trimethylstannyl-4-hexylthiophene (**2**) [21], and 2,5-bistrimethylstannylthiophene (**5**) [22] were synthesized by following the literature method. 2,5-Bistrimethylstannyl-3-hexylthiophene (**6**) was synthesized according to our recent publication [23]. [6,6]-Phenyl-C_{61}-butyric acid methyl ester ($PC_{61}BM$) and [6,6]-phenyl-C_{71}-butyric acid methyl ester ($PC_{71}BM$) were obtained from Nano-C and American Dye Source Inc., respectively. Poly (3,4-ethylenedioxythiophene):poly(styrene sulfonate) (PEDOT: PSS) (Clevios P VP AI 4083) was purchased from H.C. Stark and passed through a 0.45 μm PES syringe filter before spin-coating.

2.2. Synthesis

Synthesis of 4,7-di(4-hexylthien-2-yl)-2,1,3-benzothiadiazole (3): 4,7-Di(4-hexylthien-2-yl)-2,1,3-benzothiadiazole was prepared by modifying the literature method [24]. 4,7-Dibromo-2,1,3-benzothiadiazole (3.35 g, 0.0114 mol) and 2-trimethylstannyl-4-hexylthiophene (9.4 g, 0.0284 mol) were dissolved in 40 m*l* of anhydrous toluene. The solution was deaerated under vacuum and backfilled with N_2 gas, and this was repeated three times prior to addition of $Pd(PPh_3)_2Cl_2$ catalyst (400 mg, 0.00057 mol). The solution was allowed to react at 110 °C for 24 h under nitrogen atmosphere. The solvent was removed under a reduced pressure, and then the residue was purified by column chromatography on silica gel (1:3 chloroform/hexane as eluent) to yield a red compound which solidifies upon standing. Yield: 4.94 g (93%). ^{1}H NMR (300 MHz, $CDCl_3$): δ (ppm) 7.95 (dd, 2H), 7.80 (s, 2H), 7.05 (dd, 2H), 2.68 (t, 4H), 1.70 (m, 4H), 1.23-1.51 (m, 12H), 0.92 (t, 6H). ^{13}C NMR (75 MHz, $CDCl_3$): δ (ppm) 153.09, 139.70, 128.35, 127.90, 127.25, 126.42, 126.09, 34.31, 31.88, 29.72, 24.63, 22.29, 14.14. Elemental Anal. Calcd for $C_{26}H_{32}N_2S_3$ (%): C, 66.67; H, 6.84; N, 5.98; S, 20.51. Found (%): C, 66.31; H, 6.93; N, 6.00; S, 20.86.

Synthesis of 4,7-bis(5-bromo-(4-hexylthien-2-yl)-2,1,3-benzothiadiazole (4): The compound **3** (2.02 g, 0.0043 mol) was dissolved in 30 m*l* of THF, to which N-bromosuccinimide (NBS) (1.612 g, 0.0091 mol) was added in the dark. After stirring the mixture at room temperature for 3 h, 90 m*l* of n-hexane was added into the mixture, and then the precipitate was filtered. The filtrate was extracted with ether, and the organic layer was washed with brine and dried over anhydrous magnesium sulfate. Evaporation of the solvent yielded the product as a red compound which solidifies upon standing. Yield: 2.40 g (89%). ^{1}H NMR (300 MHz, $CDCl_3$): δ (ppm) 7.77 (s, 2H), 7.66 (s, 2H), 2.65 (t, 4H), 1.66 (m, 4H), 1.31-1.43 (m, 12H), 0.92 (t, 6H). ^{13}C NMR (75 MHz, $CDCl_3$): δ (ppm) 152.09, 142.90, 138.35, 127.90, 125.15, 124.42, 111.59, 34.22, 31.90, 30.04, 23.78, 21.88, 14.13. Elemental Anal. Calcd for $C_{26}H_{32}N_2S_3Br_2$ (%): C, 49.86; H, 4.79; N, 4.47; S, 15.36. Found (%): C, 49.85; H, 4.78; N, 4.50; S, 15.30.

Synthesis of poly(3,3''-dihexyl-2,2':5',2''-terthiophene-alt-2,1,3-benzothiadiazole) (P1): Under nitrogen atmosphere, monomer **4** (384 mg, 0.613 mmol) and **5** (251.1 mg, 0.613 mmol) were dissolved in 20 m*l* of anhydrous 1,2-dichlorobenzene. The solution was flushed with N_2 for 20 min, and then 21.6 mg of $Pd(PPh_3)_2Cl_2$ was added. After the reaction mixture was stirred at 120 °C for 48 h, the polymer was precipitated by addition of 80 m*l* of methanol. The crude product was filtered through a Soxhlet thimble, and then subjected to Soxhlet extraction with methanol, hexane, acetone, and chloroform. The polymer was recovered from the chloroform fraction, and precipitated into methanol/acetone (1:1 v/v) to afford the product as black solid. Yield: 203.9 mg (63%). ^{1}H NMR (300 MHz, $CDCl_3$): δ (ppm) 6.51-8.02 (br, 5H), 2.07-2.87 (br, 4H), 1.09-1.72 (m, 16H), 0.92 (s, 6H). Elemental Anal. Calcd for $C_{30}H_{32}N_2S_4$ (%): C, 65.58; H, 5.83; N, 5.10; S, 23.38. Found (%): C, 65.52; H, 6.00; N, 5.18; S, 23.00.

Synthesis of poly(3,3'3''-trihexyl-2,2':5',2''-terthiophene-alt-2,1,3-benzothiadiazole) (P2): The polymerization process was the same as that of **P1**, except that the monomer **6** was used instead of **5**. Yield: 146.7 mg (55%). ^{1}H NMR (300 MHz, $CDCl_3$): δ(ppm) 7.92-8.13 (m, 2H), 7.80 (s, 2H), 7.15 (s, 1H), 2.68 (m, 6H), 1.17-1.79 (m, 24H), 0.93 (m, 9H). Elemental Anal. Calcd for $C_{36}H_{44}N_2S_4$ (%): C, 68.34; H, 6.96; N, 4.43; S, 20.27. Found (%): C, 68.38; H, 6.84; N, 4.40; S, 20.39.

2.3. Characterization

The chemical structures of materials used in this study were identified by ^{1}H NMR (Avance DPX-300). Elemental analysis was performed on EA1110 (CE Instrument) elemental analyzer. Molecular weight and its distribution were measured by gel permeation chromatography (Waters) equipped with a Waters 2414 refractive index detector using THF as an eluent, where the columns were calibrated against standard polystyrene samples. The optical absorption spectra were obtained by UV-Vis spectrophotometer (Lambda 25, Perkin Elmer). Cyclic voltammetry experiments were carried out on potentiostat/galvanostat (VMP 3, Biologic) in an electrolyte solution of 0.1 M tetrabutylammonium hexafluorophosphate (Bu_4NPF_6) in dichloromethane. Three-electrode cell was used for all experiments. Platinum wires (Bioanalytical System Inc.) were used as both counter and working electrodes, and

silver/silver ion (Ag in 0.1 M $AgNO_3$ solution, Bioanalytical System Inc.) was used as a reference electrode. Differential scanning calorimetry (DSC) measurements were performed under nitrogen at a heating rate of 10 °C/min (DSC 2920, TA Instruments). X-ray diffraction (XRD) pattern was obtained from X-ray diffractometer (M18XHF-SRA, McScience) using CuKα radiation (λ=1,5418 Å) at a scan rate of 2 °/min. TEM observations were performed on a JEOL JEM1010 at an accelerating voltage of 80 kV.

2.4. Fabrication and Characterization of Photovoltaic Devices

Polymer solar cells were fabricated on ITO glass cleaned by stepwise sonication in acetone and IPA, followed by O_2 plasma treatment for 10 min. PEDOT:PSS was spin-coated on the ITO glass at 4000 rpm for 1 min and annealed at 150 °C for 30 min to yield 40 nm thick film. A mixture of **P1** (or **P2**) and PCBM were dissolved in anhydrous dichlorobenzene (30 mg/m*l*), and spin-coated on the top of the ITO/PEDOT:PSS film at 700-800 rpm for 60 sec. The typical thickness of the active layer was 130-150 nm. Aluminum (100 nm) was evaporated under vacuum lower than 10^{-6} Torr on the top of active layer through a shadow mask. The effective area of cell was ca. 4 mm^2. The current-voltage (J-V) curves of the device were obtained on a computer-controlled Keithley 4200 source measurement unit under AM 1.5G (100 mW/cm^2) simulated by an Oriel solar simulator (Oriel 91160A). The light intensity was calibrated using a NREL-certified photodiode prior to each measurement. The external quantum efficiency (EQE) was measured using Polaronix K3100 IPCE measurement system (McScience). The light intensity at each wavelength was calibrated with a standard single-crystal Si cell.

3. Results and Discussion

3.1. Synthesis and Characterization

The synthetic route for preparation of monomers and polymers are shown in *Figure* 1. Considering that the number of hexyl groups attached to the thiophene rings of the monomers may influence the properties of the resulting polymers, two different monomers (**5** and **6** in *Figure* 1) were used as a building block of copolymers. The palladium-catalyzed Stille coupling reaction was employed to synthesize alternating copolymer of thiophene and benzothiadiazole which are electron-donating and electron-withdrawing unit, respectively. All the polymers in this study are highly soluble in common organic solvent such as chloroform, chlorobenzene, and dichlorobenzene at room temperature. The number-average molecular weight (M_n) and polydispersity index (PDI) of **P1** and **P2** are listed in *Table* 1. The molecular weight of **P2** is low probably due to the steric hindrance of the 3'-hexyl group in the monomer **6** which causes poor reactivity toward palladium-catalyzed polymerization reaction.

3.2. Optical Properties

The absorption spectra of the two polymers in chloroform solution and thin film are shown in *Figure* 2(a) and 2(b),

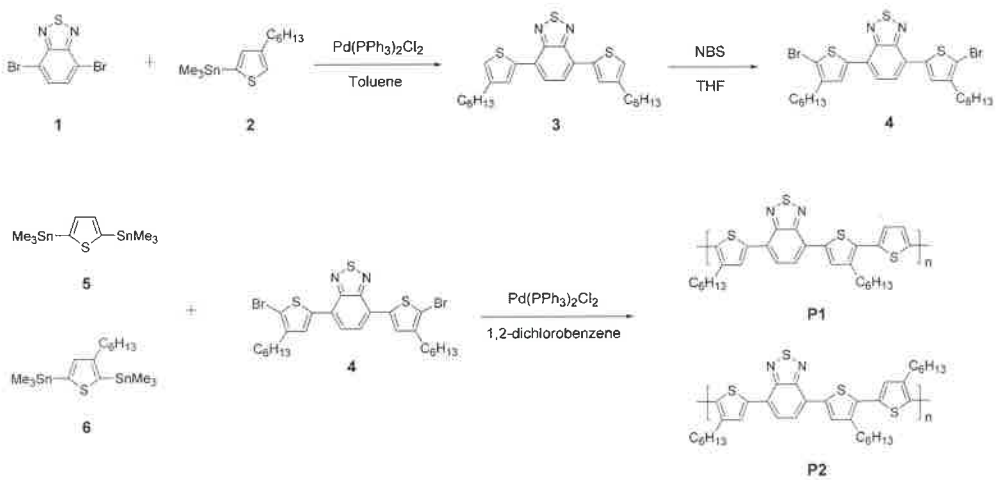

Figure 1. Synthetic route of alternating copolymers.

Table 1. Characteristics of polymers

Polymer	M_n (kg/mol)	PDI	Absorption		E_g (opt)[a] (eV)	HOMO (eV)	LUMO (eV)	E_g (ec)[b] (eV)
			λ_{max}($CHCl_3$) (nm)	λ_{max}(film) (nm)				
P1	27.8	1.61	560	657	1.52	−5.29	−3.40	1.89
P2	8.2	1.55	518	544	1.70	−5.27	−3.32	1.95

[a]Determined from the onset of UV-Vis absorption spectra and [b]calculated from the cyclic voltammetry.

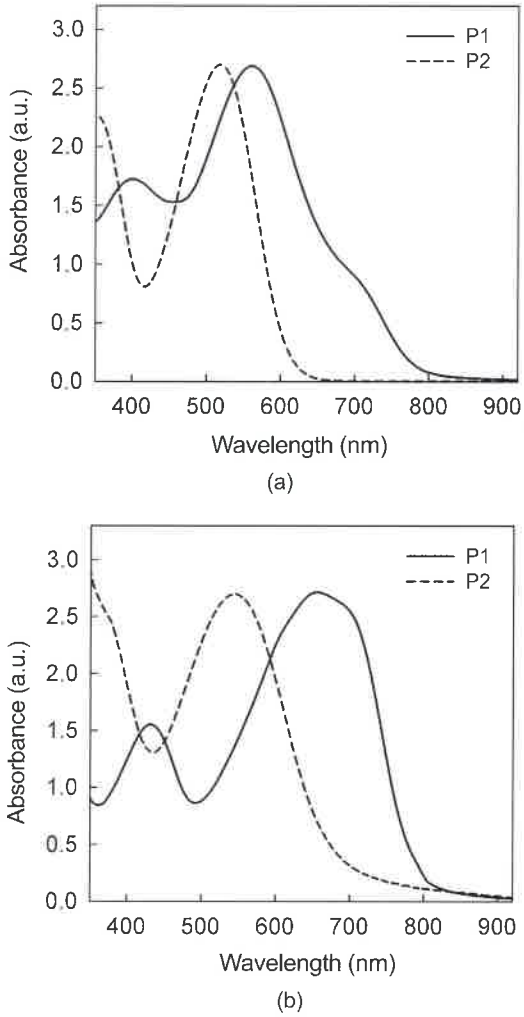

Figure 2. UV-Vis absorption spectra of the copolymers in chloroform solution (a) and solid state (b).

respectively. Both of the two polymers showed two absorption peaks, which is a common feature of donor-acceptor type copolymers [25,26]. The absorption peak at shorter wavelength is attributed to π-π^* transition of thiophene units, while the absorption peak at longer wavelength corresponds to the intramolecular charge transfer from the donor to the acceptor. It is noted that the absorption of **P1** is much broader than that of **P2**. Interestingly, the absorption spectrum of **P1** in solution exhibits a shoulder peak at long wavelength region due to the vibronic coupling associated with molecular rigidity. Particularly, when the maximum absorption wavelengths of the polymers in solution are compared with those in solid state (*Figure* 2(a) vs. *Figure* 2(b)), it reveals that **P1** shows a pronounced red shift of 97 nm from solution to solid state. This is probably due to the decreased steric repulsion of hexyl side groups of **P1** which has one unsubstituted thiophene in the repeating unit, providing other hexyl side groups with torsion-releasing space. For this reason, **P1** may have planar

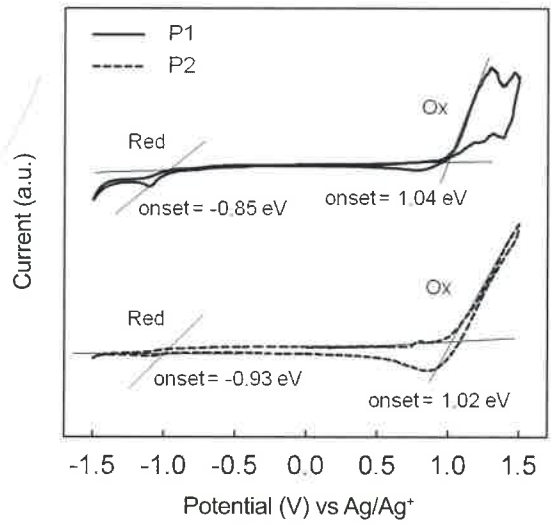

Figure 3. Cyclic voltammograms of **P1** and **P2**.

structure and thus easily aggregate in the solid state. The optical bandgaps (E_g(opt)) as determined from the onset of the absorption spectra of **P1** and **P2** are 1.52 eV and 1.70 eV, respectively, which are very close to the ideal bandgap (1.5 eV) [27] of polymer solar cells.

3.3. Electrochemical Properties

The electrochemical data of all the polymers are obtained from the oxidation and reduction cyclic voltammograms, as shown in *Figure* 3, and are summarized in *Table* 1. The HOMO energy levels of the polymers can be calculated using the equation: HOMO=$-[E_{ox}-E_{1/2}$(ferrocene)+4.8] V, where E_{ox} is the onset oxidation potential of polymer and $E_{1/2}$ (ferrocene) is the onset oxidation potential of ferrocene versus Ag/Ag^+. The LUMO energy levels can be estimated by using the equation: LUMO=$-[E_{red}-E_{1/2}$(ferrocene)+4.8] V, where E_{red} is the onset reduction potential of polymer. The estimated HOMO and LUMO energy levels of **P1** are −5.29 eV and −3.40 eV, and those of **P2** are −5.27 eV and −3.32 eV, respectively, from which the electrochemical bandgaps (E_g(ec)) for each polymer can be determined. Since the open circuit voltage (V_{oc}) of polymer solar cells is linearly dependent on the difference between the HOMO level of electron donor and the LUMO level of electron acceptor, low HOMO level of the donor polymer results in high V_{oc} of resulting polymer solar cells. Considering that a LUMO-LUMO offset of 0.3~0.4 eV is necessary for efficient electron transfer from polymer to $PC_{61}BM$ [28], it is expected that exciton can be easily dissociated at the interface between the polymers and $PC_{61}BM$ because the LUMO levels of the polymers are much higher than that of $PC_{61}BM$ (−4.0 eV). Judging from the electrochemical characteristics, it is expected that the polymers synthesized in this study are promising donor materials for photovoltaic devices.

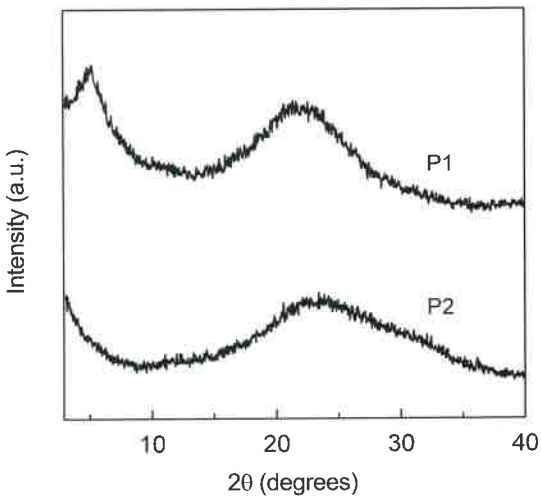

Figure 4. Powder X-ray diffractograms of **P1** and **P2**.

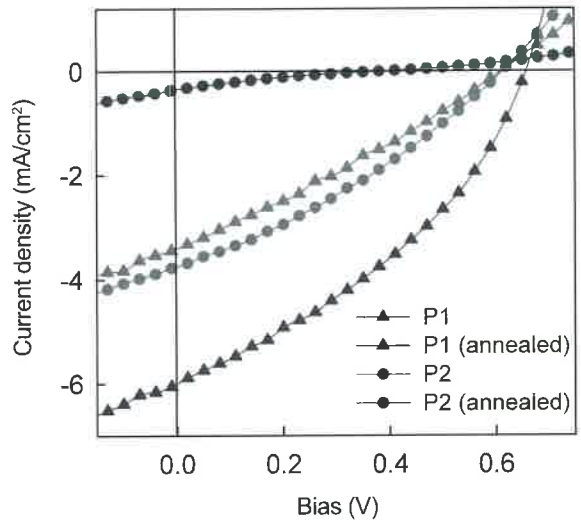

Figure 5. Current-voltage (J-V) characteristics of photovoltaic devices based on **P1**:$PC_{61}BM$ (1:4 w/w) (a) and **P2**:$PC_{61}BM$ (1:3 w/w) (b).

3.4. XRD Analysis

To investigate the molecular organization of the polymers, the XRD patterns were obtained from powdered samples of polymers. The peaks around 23 ° for both polymers can be assigned to the face-to-face distance of the aromatic groups in the polymer chains. Particularly, **P1** shows a distinct diffraction peak at 2θ=5.2 ° corresponding to the *d*-spacing value of 16.3 Å which is assigned to the interchain spacing between polymer main chains, where hexyl groups are segregated similar to other conjugated polymers with side groups [7]. Since the number of hexyl groups in the repeating unit of **P1** is smaller than that of **P2**, the unsubstituted thiophene unit in **P1** may provide sufficient space to facilitate interdigitation of side chains as above mentioned. These results are consistent with DSC studies (*Figure* S3 in Supporting Information), where **P1** shows melting peak at 207 °C and cold crystallization peak at 204 °C, while **P2** does not show the thermal transition. It should be mentioned here that Yue *et al.* [11] recently synthesized a low-bandgap polymer similar to **P1** which has dodecyl side groups in the thiophene units, reporting that the polymer has totally amorphous nature. Unlike their report, however, we could induce effectively the intermolecular packing of the polymer by reducing the length of alkyl side groups from dodecyl to hexyl.

3.5. Photovoltaic Properties

The polymer solar cells were fabricated with layered configuration of glass/ITO/PEDOT:PSS/polymer:PCBM/Al. The current-voltage characteristics of photovoltaic devices with two different polymers, **P1** and **P2**, are shown in *Figure* 5, and the photovoltaic parameters are summarized in *Table* 2. It is worth noting that the V_{oc} of **P1** and **P2** devices are slightly higher than P3HT-based devices (~0.60 V), which is in accordance with the low-lying HOMO level of **P1** and **P2**. The as-spun devices of **P1** and **P2** exhibit nearly equal photovoltaic performance with the PCE of around 0.7%. When the devices were thermally annealed, however, these two devices showed different photovoltaic effect. The solar cells of **P1**:$PC_{61}BM$ exhibited the PCE up to 1.49% with V_{oc}= 0.66 V, J_{sc}=5.95 mA/cm^2, and FF=0.38 after thermal annealing at 170 °C for 30 min. The large increase of short-circuit current upon thermal annealing is attributed to enhanced inter-chain packing of **P1**, which facilitates enhanced charge transport through the packing direction. The fill factor (FF) was also significantly increased after thermal treatment. It is well known that the FF of the device is strongly dependent upon the series resistance (R_s) and shunt resistance (R_{sh})

Table 2. Photovoltaic parameters of devices tested under standard AM 1.5G conditions

Active layer	V_{oc} (V)	J_{sc} (mA/cm^2)	*FF*	PCE (%)	R_s (Ωcm^2)[a]	R_{sh} (Ωcm^2)[a]
P1:$PC_{61}BM$ (as spun)	0.61	3.49	0.29	0.62	230	340
P1:$PC_{61}BM$ (annealed)	0.66	5.95	0.38	1.49	12	300
P2:$PC_{61}BM$ (as spun)	0.62	3.77	0.32	0.75	45	274
P2:$PC_{61}BM$ (annealed)	0.39	0.35	0.21	0.03	629	422

[a]The series resistance, R_s, is calculated at the inverse of the slope at V_{oc} and the shunt resistance, R_{sh}, is calculated at the inverse of the slope at J_{sc}.

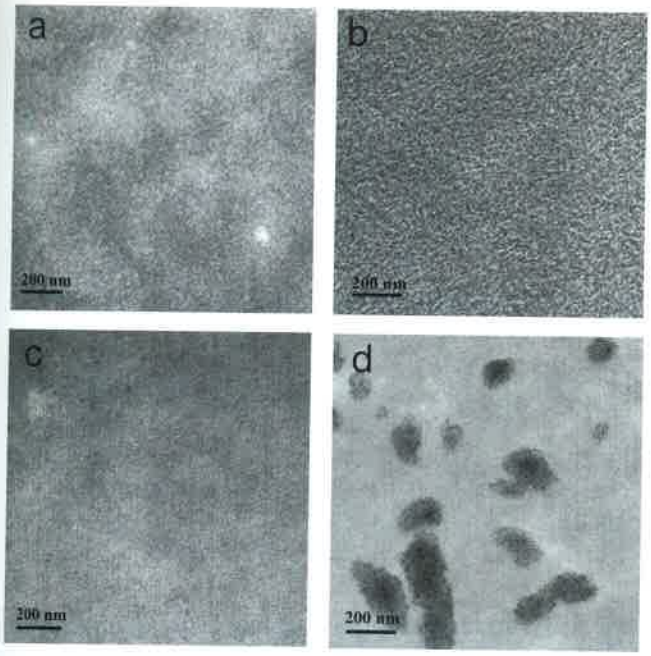

Figure 6. TEM images of **P1**:$PC_{61}BM$ blend films (a: as-spun, b: annealed) and **P2**:$PC_{61}BM$ blend films (c: as-spun, d: annealed).

[29], where R_s is closely related to the intrinsic resistance and morphology of the device, and R_{sh} is correlated with the defects in the active layer which cause recombination of charge carriers and leakage current. When the values of R_s from the J-V curves are estimated and compared before and after thermal annealing, it is realized that R_s of the thermally annealed film of **P1** is significantly lower than that of as-spun one. This decrease in R_s is attributed to the fact that the thermal treatment induces phase separation with the domain size of the exciton diffusion length (~10 nm), which will be discussed below. On the other hand, **P2**-based device showed severe loss of all the photovoltaic parameters upon thermal annealing. Although the annealing temperature was changed, the photovoltaic properties in all cases were lower than those of as-spun device of **P2**.

It is generally accepted that the morphology of the donor/acceptor blend can greatly affect the performance of photovoltaic devices [30,31]. Optimal morphology is usually characterized by nanoscale phase separation, which may reduce the probability of geminate charge recombination. When the morphology of polymer/$PC_{61}BM$ blends was characterized by TEM, the TEM images of as-spun **P1**:$PC_{61}BM$ and **P2**:$PC_{61}BM$ blend films show very uniform morphology without any characteristic feature of phase separation (*Figures* 6(a) and 6(c)), indicating good miscibility between the polymers and $PC_{61}BM$. This morphology may cause low current density because it cannot provide the pathway for charge carriers to pass through. When **P1**:$PC_{61}BM$ film was thermally annealed at 170 °C for 30 min, nanoscale phase separation was developed to afford charge carrier pathway, as shown in *Figure* 6(b), resulting in higher current density compared to as-spun device. On the contrary, when **P2**:$PC_{61}BM$ film was annealed under the same condition as **P1**:$PC_{61}BM$, macro-phase separation was observed, as shown in *Figure* 6(d). This large phase separation may aggravate the device performance.

To quantitatively investigate the effect of phase-separated morphology on the charge transport property, hole and electron mobilities were determined from the space charge limited current (SCLC) J-V curves as obtained in the dark for hole-only devices (ITO/PEDOT:PSS/polymer:$PC_{61}BM$/Au) and electron-only devices (Al/polymer:$PC_{61}BM$/Al),

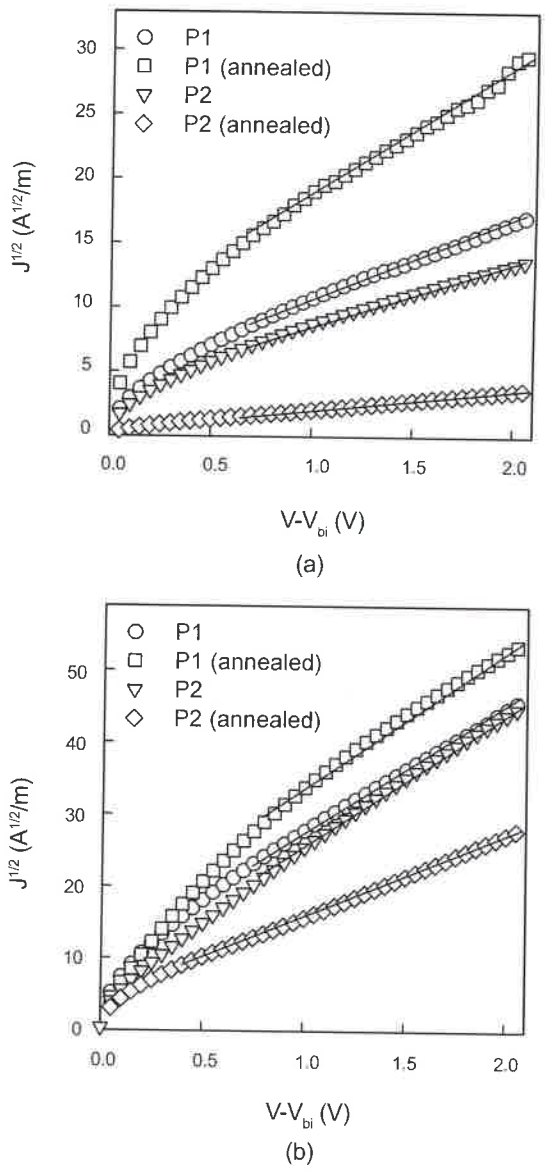

Figure 7. Dark J-V characteristics for hole-only (a) and electron-only (b) devices of **P1**:$PC_{61}BM$ and **P2**:$PC_{61}BM$. The solid lines are the best linear fit of the data points.

respectively. The SCLC behavior can be analyzed using the Mott-Gurney law [32]: $J=(9/8)\varepsilon\mu(V^2/L^3)$, where ε is the static dielectric constant of the medium, μ is the carrier mobility, $V=V_a-V_{bi}$ (V_a, the applied bias; V_{bi}, the built-in potential due to the difference in electrical contact work functions), and L is the layer thickness. The hole mobilities, determined from the slope of $J^{1/2}$ versus V, were 7.83×10^{-6} $cm^2/V\cdot s$ and 6.27×10^{-6} $cm^2/V\cdot s$ for as-spun devices of **P1** and **P2**, respectively. The annealed device of **P1** exhibited enhanced hole mobility of 1.29×10^{-5} $cm^2/V\cdot s$, showing 65% increase compared to that of device without thermal treatment, while the hole mobility of **P2** device was rather decreased to 1.98×10^{-6} $cm^2/V\cdot s$ after thermal annealing. The electron mobilities of four devices were almost same: as-spun **P1**, 2.27×10^{-5} $cm^2/V\cdot s$; annealed **P1**, 2.68×10^{-5} $cm^2/V\cdot s$; as-spun **P2**, 2.14×10^{-5} $cm^2/V\cdot s$; annealed **P2**, 1.35×10^{-5} $cm^2/V\cdot s$. It is noted that the annealed device of **P1** shows a balanced hole and electron mobility (1.29×10^{-5} $cm^2/V\cdot s$ versus 2.68×10^{-5} $cm^2/V\cdot s$) while that of **P2** shows large discrepancy between hole and electron mobility (1.98×10^{-6} $cm^2/V\cdot s$ versus 1.35×10^{-5} $cm^2/V\cdot s$).

To improve the photon harvesting capability of the active layer, $PC_{71}BM$ was used as an electron acceptor in the blend. When $PC_{71}BM$ is blended with **P1**, the **P1**:$PC_{71}BM$ (1:4 w/w) device exhibits a promising PCE of 2.19% with V_{oc}=0.70 V, J_{sc}=8.95 mA/cm^2, and FF=0.35 after thermal annealing at 170 °C for 30 min (*Figure* 8, *Table* 3). The large increase in J_{sc} reflects enhanced photon harvesting ability of the active layer when $PC_{61}BM$ is replaced by $PC_{71}BM$. When the external quantum efficiency (EQE) of $PC_{61}BM$ based devices are compared with those of $PC_{71}BM$ based devices, as can be seen in *Figure* 9, it reveals that the $PC_{71}BM$-based devices exhibit larger EQE than $PC_{61}BM$-based devices in the wavelength from 350 nm to 600 nm due to additional light absorption of $PC_{71}BM$ in that region. Further device optimization such as interface engineering between active layer and cathode, and control of film morphology using mixed solvent is needed to improve the device performance.

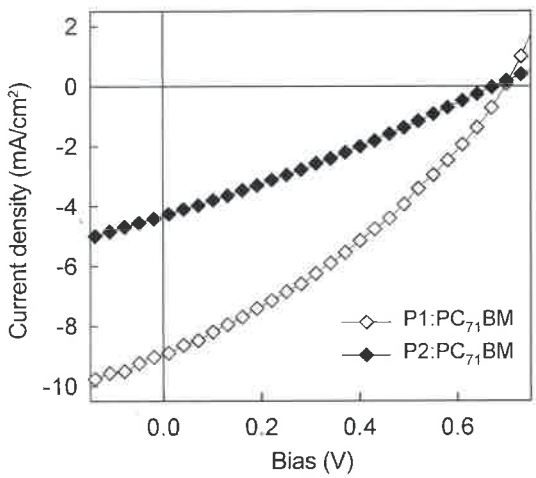

Figure 8. J-V curves of photovoltaic devices using $PC_{71}BM$ as an electron acceptor.

Table 3. Photovoltaic parameters of devices with $PC_{71}BM$ as an acceptor

Active layer	V_{oc} (V)	J_{sc} (mA/cm^2)	*FF*	PCE (%)
P1:$PC_{71}BM$	0.70	8.95	0.35	2.19
P2:$PC_{71}BM$	0.68	4.33	0.31	0.91

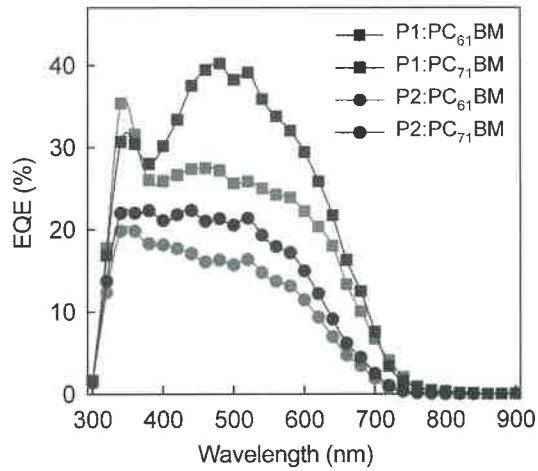

Figure 9. External quantum efficiency spectra of polymer/PCBM solar cells.

4. Conclusions

We have synthesized two conjugated D-A low-bandgap alternating copolymers composed of oligothiophene and benzothiadiazole via the Stille coupling polymerization. It has been found that the optical, structural, and photovoltaic properties of the copolymers are strongly dependent upon the number of side groups in the repeating unit of polymer chain. **P1** has better interchain packing as compared with **P2**, which results in enhanced charge carrier mobility and power conversion efficiency of 2.19%. This result indicates that low-bandgap polymers with high degree of interchain packing should be synthesized for high performance polymer solar cells by fine-tuning of the substitution pattern of side group.

Acknowledgment: The authors thank the Ministry of Education, Science and Technology (MEST), Korea for financial support through the Global Research Laboratory (GRL) program.

Supporting information

^{1}H NMR and DSC of polymers, and detailed J-V curves of the polymer solar cells. This material is available free of charge via the internet.

References

1. G. Yu, J. Gao, J. C. Hummelen, F. Wudl, and A. J. Heeger, "Polymer Photovoltaic Cells: Enhanced Efficiencies via a Network of Internal Donor-Acceptor Heterojunctions", Science, 1995, 270, 1789-1791.
2. K. M. Coakley and M. D. McGehee, "Conjugated Polymer Photovoltaic Cells", Chem Mater, 2044, 16, 4533-4542.
3. V. D. Mihailetchi, L. J. A. Koster, P. W. M. Blom, C. Melzer, B. de Boer, J. K. J. van Duren, and R. A. J. Janssen, "Compositional Dependence of the Performance of Poly(p-phenylene vinylene): Methanofullerene Bulk-Heterojunction Solar Cells", Adv Funct Mater, 2005, 15, 795-801.
4. H. Xin, G. Ren, F. S. Kim, and S. A. Jenekhe, "Bulk Heterojunction Solar Cells from Poly(3-butylthiophene)/ Fullerene Blends: In Situ Self-Assembly of Nanowires, Morphology, Charge Transport, and Photovoltaic Properties", Chem Mater, 2008, 20, 6199-6207.
5. G. Li, V. Shrotriya, J. Huang, Y. Yao, T. Moriarty, K. Emery, and Y. Yang, "High-efficiency Solution Processable Polymer Photovoltaic Cells by Self-organization of Polymer Blends" Nat Mater, 2005, 4, 864-868.
6. W. L. Ma, C. Y. Yang, X. Gong, K. H. Lee, and A. J. Heeger, "Thermally Stable, Efficient Polymer Solar Cells with Nanoscale Control of the Interpenetrating Network Morphology", Adv Funct Mater, 2005, 15, 1617-1622.
7. N. Blouin, A. Michaud, D. Gendron, S. Wakim, E. Blair, R. Neagu-Plesu, M. Bellette, G. Durocher, Y. Tao, and M. Leclerc, "Toward a Rational Design of Poly(2,7-Carbazole) Derivatives for Solar Cells", J Am Chem Soc, 2008, 130, 732-742.
8. J. Y. Kim, Y. Qin, D. M. Stevens, O. Ugurlu, V. Kalihari, M. A. Hillmyer, and C. D. Frisbie, "Low Band Gap Poly(thienylene vinylene)/Fullerene Bulk Heterojunction Photovoltaic Cells", J Phys Chem C, 2009, 113, 10790-10797.
9. J. Kim, S. H. Park, S. Cho, Y. Jin, J. Kim, I. Kim, J. S. Lee, J. H. Kim, H. Y. Woo, K. Lee, and H. Suh, "Low-bandgap Poly(4H-cyclopentadef]phenanthrene) Derivatives with 4,7-dithienyl-2,1,3-benzothiadiazole Unit for Photovoltaic cells" , Polymer, 2010, 51, 390-396.
10. Y. Zhang, S. K. Hau, H. Yip, Y. Sun, O. Acton, and A. K. Jen, "Efficient Polymer Solar Cells Based on the Copolymers of Benzodithiophene and Thienopyrroledione", Chem Mater, 2010, 22, 2696-2698.
11. W. Yue, Y. Zhao, H. Tian, D. Song, Z. Xie, D. Yan, Y. Geng, and F. Wang, "Poly(oligothiophene-alt-benzothiadiazole)s: Tuning the Structures of Oligothiophene Units Toward High-Mobility "Black" Conjugated Polymers", Macromolecules, 2009, 42, 6510-6518.
12. J. Hou, H. Chen, S. Zhang, and Y. Yang, "Synthesis and Photovoltaic Properties of Two Benzo1,2-b:3,4-b']dithiophene-Based Conjugated Polymers", J Phys Chem C, 2009, 113, 21202-21207.
13. J. Tsai, W. Lee, W. Chen, C. Yu, G. Hwang, and C. Ting, "New Two-Dimensional ThiopheneAcceptor Conjugated Copolymers for Field Effect Transistor and Photovoltaic Cell Applications", Chem Mater, 2010, 22, 3290-3299.
14. S. H. Park, A. Roy, S. Beaupré, S. Cho, N. Coates, J. S. Moon, D. Moses, M. Leclerc, K. Lee, and A. J. Heeger, "Bulk Heterojunction Solar Cells with Internal Quantum Efficiency Approaching 100%", Nat Photonics, 2009, 3, 297-302.
15. M. Zhang, H. N. Tsao, W. Pisula, C. Yang, A. K. Mishra, and K. Müllen, "Field-Effect Transistors Based on a BenzothiadiazoleCyclopentadithiophene Copolymer", J Am Chem Soc, 2007, 129, 3472-3473.
16. C. Yang, S. Cho, R. C. Chiechi, W. Walker, N. E. Coates, D. Moses, A. J. Heeger, and F. Wudl, "VisibleNear Infrared Absorbing Dithienylcyclopentadienone-Thiophene Copolymers for Organic Thin-Film Transistors", J Am Chem Soc, 2008, 130, 16524-16526.
17. J. Lu, F. Liang, N. Drolet, J. Ding, Y. Tao, and R. Movileanu, "Crystalline Low Band-gap Alternating Indolocarbazole and Benzothiadiazole-cored Oligothiophene Copolymer for Organic Solar Cell Applications", Chem Commun, 2008, 42, 5315-5317.
18. H. Xin, X. Guo, F. S. Kim, G. Ren, M. D. Watson, and S. A. Jenekhe, "Efficient Solar Cells Based on a New Phthalimide-based Donor-acceptor Copolymer Semiconductor: Morphology, Charge-transport, and Photovoltaic Properties", J Mater Chem, 2009, 19, 5303-5310.
19. Y. Li, H. Li, B. Xu, Z. Li, F. Chen, D. Feng, J. Zhang, and W. Tian, "Molecular Structure-property Engineering for Photovoltaic Applications: Fluorene-acceptor Alternating Conjugated Copolymers with Varied Bridged Moieties", Polymer, 2010, 51, 1786-1795.
20. A. P. Zoombelt, M. Fonrodona, M. M. Wienk, A. B. Sieval, J. C. Hummelen, and R. A. J. Janssen, "Photovoltaic Performance of an Ultrasmall Band Gap Polymer", Org Lett, 2009, 11, 903-906.
21. E. Bundgaard, and F. C. Krebs, "Low-band-gap Conjugated Polymers Based on Thiophene, Benzothiadiazole, and Benzobis (thiadiazole)", Macromolecules, 2006, 39, 2823-2831.
22. Y. Wei, Y. Yang, and J. Yeh, "Synthesis and Electronic Properties of Aldehyde End-Capped Thiophene Oligomers and Other α,ω-Substituted Sexithiophenes", Chem Mater, 1996, 8, 2659-2666.
23. Y. Lee, T. P. Russell, and W. H. Jo, "Synthesis and Photovoltaic Properties of Low-bandgap Alternating Copolymers Consisting of 3-hexylthiophene and [1,2,5]thiadiazolo[3,4-g]quinoxaline Derivatives", Org Electron, 2010, 11, 846-853.
24. Q. Hou, Q. Zhou, Y. Zhang, W. Yang, R. Yang, and Y. Cao, "Synthesis and Electroluminescent Properties of High-Efficiency Saturated Red Emitter Based on Copolymers

from Fluorene and 4,7-Di(4-hexylthien-2-yl)-2,1,3-benzothiadiazole", Macromolecules, 2004, 37, 6299-6305.
25. J. Yang, Q. Hou, W. Yang, C. Zhang, and Y. Cao, "Deep-Red Electroluminescent Polymers: Synthesis and Characterization of New Low-Band-Gap Conjugated Copolymers for Light-Emitting Diodes and Photovoltaic Devices", Macromolecules, 2005, 38, 244-253.
26. C. Kanimozhi, P. Balraju, G. D. Sharma, and S. Patil, "Synthesis of Diketopyrrolopyrrole Containing Copolymers: A Study of Their Optical and Photovoltaic Properties", J Phys Chem B, 2010, 114, 3095-3103.
27. M. C. Scharber, D. Muhlbacher, M. Koppe, P. Denk, C. Waldauf, A. J. Heeger, and C. J. Brabec, "Design Rules for Donors in Bulk-Heterojunction Solar Cells-Towards 10% Energy-Conversion Efficiency", Adv Funct Mater, 2006, 18, 789-794.
28. A. P. Zoombelt, M. Fonrodona, M. G. R. Turbiez, M. M. Wienk, and R. A. J. Janssen, "Synthesis and Photovoltaic Performance of a Series of small Band Gap Polymers", J Mater Chem, 2009, 19, 5336-5342.
29. S. Günes, H. Neugebauer, and N. S. Sariciftci, "Conjugated Polymer-Based Organic Solar Cells", Chem Rev, 2007, 107, 1324-1338.
30. Z. Peet, J. Y. Kim, N. E. Coates, W. I. Ma, D. Moses, A. J. Heeger, and G. C. Bazan, "Efficiency Enhancement in Low-bandgap Polymer Solar Cells by Processing with Alkane Dithiols", Nat Mater, 2007, 6, 497-500.
31. D. M. Stevens, Y. Qin, M. A. Hillmyer, and C. D. Frisbie, "Enhancement of the Morphology and Open Circuit Voltage in Bilayer Polymer/Fullerene Solar Cells", J Phys Chem C, 2009, 113, 11408-11415.
32. P. N. Murgatroyd, "Theory of Space-charge-limited Current Enhanced by Frenkel Effect", J Phys D: Appl Phys, 1970, 3, 151-156.